1. In the calculations, the Mach number M was 0.73 and the angle of attack α was 2.8 deg. These are the same (corrected) conditions used by Coakley and by King. Included in Fig. 2 is a table of the lift and drag coefficients (C_L and C_D, respectively) for the calculations and the experiment. In all calculations, wall properties were used for y^+ in the van Driest damping term (i.e., $y^+ = y\rho_w u_\tau/\mu_w$). No pressure-gradient corrections for A^+ were applied.

In the *new* Johnson-King results, the diffusion term of that model was set to zero when the parameter σ of the model was less than 1. For the RAE 2822 airfoil test cases 6, 9, and 10, this change had little effect on computed results. But for the NACA 0012 airfoil, this change had a pronounced effect on predicted shock location. The original purpose of the diffusion term was to achieve better model performance in regions of flow recovery (i.e., regions where $\sigma > 1$). At the time, it was thought that the modeled diffusion term had a negligible influence in regions where σ was less than unity. Such appears not always to be the case. Considering that the validity of this term is far from established, the judicious approach is to include it only where it is known to improve the computed results—regions where σ exceeds unity.

It should be noted that the pressure rise across the shock predicted by the Johnson-King model is in better agreement with experiment than that predicted with the Cebeci-Smith model. The weaker shock is a result of a more rapid boundary-layer growth in the shock region.

For the Cebeci-Smith model solution shown in Fig. 2, the larger of the two quantities u_τ and $\sqrt{\rho_m/\rho_w}\,u_m$ was also used in the van Driest damping term. The use of simply $|u_\tau|$ instead, as has commonly been done in the implementation of the Cebeci-Smith and Baldwin-Lomax models, does not appear to be appropriate since it predicts early separation. Moreover, because of lower predicted wall shear levels on the aft section of the airfoil, it results in slower boundary-layer growth. This is accompanied by an increase in lift and a shock location that is slightly more aft in spite of the presence of separation. For the Cebeci-Smith model, C_L increases from 0.825 to 0.836 when $|u_\tau|$ alone is used in the damping term.

Because of the presence of wind-tunnel wall effects in this experiment, there is some question as to what freestream conditions should be used in the calculations. Lift and drag levels closer to those of the experiment are obtained with both the proposed modified Johnson-King model and the Cebeci-Smith modes for $M = 0.734$ and $\alpha = 2.65$ deg. A comparison of pressure distributions and a table of C_L and C_D for these conditions are presented in Fig. 3.

References

[1]Coakley, T. J., "Numerical Simulation of Viscous Transonic Airfoil Flows," AIAA Paper 87-0416, Jan. 1987.

[2]King, L. S., "A Comparison of Turbulence Closure Models for Transonic Flows About Airfoils," AIAA Paper 87-0418, Jan. 1987.

[3]Johnson, D. A., and King, L. S., "A Mathematically Simple Turbulence Closure Model for Attached and Separated Turbulent Boundary Layers," *AIAA Journal*, Vol. 23, Nov. 1985, pp. 1684–1692.

[4]Johnson, D. A., "Transonic Separated Flow Predictions with an Eddy-Viscosity/Reynolds-Stress Closure Model," *AIAA Journal*, Vol. 25, Feb. 1987, pp. 252–259.

[5]Cebeci, T., and Smith, A. M. O., *Analysis of Turbulent Boundary Layers*, Academic, New York, 1974, Chap. 6.

[6]Baldwin, B. S., and Lomax, H., "Thin-Layer Approximation and Algebraic Model for Separated Turbulent Flows," AIAA Paper 78-257, Jan. 1978.

[7]Cook, P. H., McDonald, M. A., and Firmin, M. C. P., "Aerofoil RAE 2822—Pressure Distributions, and Boundary Layer and Wake Measurements," AGARD AR-138, May 1979.

[8]Clauser, F. H., "The Turbulent Boundary Layer," *Advances in Applied Mechanics*, edited by H. L. Dryden and T. von Kármán, Vol. 4, Academic, New York, 1956, pp. 1–51.

[9]Galbraith, R. A. McD., Sjolander, S., and Head, M. R., "Mixing Length in the Wall Region of Turbulent Boundary Layers," *Aeronautical Quarterly*, Vol. 28, May 1977, pp. 97–110.

Characteristics of Hot-Film Anemometers for Use in Hypersonic Flows

Anthony Demetriades* and Scott G. Anders†
Montana State University, Bozeman, Montana 59717

TURBULENCE measurements in high-speed flows have been traditionally conducted with the hot-wire anemometer.[1] Because of the severe compressibility effects and the frequency response requirements, hot-wire signals in such flows can be interpreted only by making assumptions on the nature of the turbulence and then only by resorting to analog or digital response restoration schemes.[2] Among users of hot wires at high speeds, however, the major issue is the structural endurance of the hot wire in high-temperature, high-dynamic-pressure flows, often laden with destructive projectiles in the form of dust or liquid particles. In such an environment, the endurance problem should be eased for "hot-film" anemometers, which replace the fragile wire by a thin metallic film deposited on a rigid substrate. Some characteristics of such hot films are described in this Note.

Although hot-film anemometer probes have already been used at hypersonic speeds,[3] most of the reports on their use, and the choice one has among commercially available models, concerns applications in low-speed flows of gases and liquids[4] and low-to-moderate temperatures. Furthermore, the low-speed research gives very scant data on those basic hot-film properties that could guide the development for high-speed, high-temperature applications, long before issues of frequency response are addressed. In the present research, in addition to developing hot-film sensors capable of continuous exposure to high temperatures, measurements of the thermometric and heat-transfer properties of such typical films were made.

The present films consisted of a 0.05-cm × 0.18-cm film of platinum deposited on the stagnation line of a wedge-shaped glaze bead positioned at the tip of a 10-cm long, 0.25-cm-diam, twin-bore alumina tube.[5] Temperature endurance of each probe was checked during the fabrication process, which cycled each probe to 760°C, and in subsequent electrical stability tests in which the probe resistance was observed continuously at 730°C, typically for an hour. Probes of this design have also operated for several hours on end in the Montana State University Mach 3 wind tunnel and in the Mach 8 tunnel B of the Arnold Engineering Development Center (AEDC), where dynamic and temperature loads of 20.7 kPa and 425°C are encountered. Destructive tests pushing the film overheat to 90%, and film temperatures to 760°C have also reinforced confidence in film-probe durability.

Resistivity calibrations of these probes are routinely done in a controlled oven to determine the film resistance R dependence on the ambient temperature as represented by the "first" and "second" resistivity coefficients α and β:

$$R = R_r\left[1 + \alpha(T - T_r) + \beta(T - T_r)^2\right] \tag{1}$$

where R_r and T_r are reference conditions. In hot-wire anemometry, which historically has dealt with lower temperatures, there is little interest in or use of the β coefficient. In the present work, the calibration interval extended to 600°C to anticipate the use of the probes in hypersonic flows. As Fig. 1 shows, the resistance variation with ambient temperature is

Received Sept. 22, 1989; revision received Dec. 7, 1989; accepted for publication Dec. 19, 1989.

*Professor, Mechanical Engineering Department.

†Graduate Student, Mechanical Engineering Department.

where R_r and T_r are reference conditions. In hot-wire anemometry, which historically has dealt with lower temperatures, there is little interest in or use of the β coefficient. In the present work, the calibration interval extended to 600°C to anticipate the use of the probes in hypersonic flows. As Fig. 1 shows, the resistance variation with ambient temperature is not linear, and thus β is significant. Ten different probes, subjected to eighteen calibrations, showed an average α of 0.0029 ± 0.00009 1/°C and an average β of $-5.8 \times 10^{-7} \pm 0.832 \times 10^{-7}$ 1/°C^2. These standard deviations of 3% and 14%, respectively, speak highly of the predictability of α and β for this type of probe. The values of α and β are also reasonably close to those quoted by Hinze[6] for platinum ($\alpha = 0.0035$ 1/°C, $\beta = -5.5 \times 10^{-7}$ 1/°C^2).

The electric power W dissipated by radiation-free thermal sensors (wires, film) is related to the thermal conductivity of the surrounding fluid k and its temperature gain $T - T_e$ above the zero-power condition by

$$W = k_e \bar{N}(T - T_e) \tag{2}$$

where $\bar{N}$ is a dimensional Nusselt number conveniently including geometric and numerical factors, and $(\ )_e$ denotes the zero-power condition ($\bar{N}$ includes conduction losses for films and finite wires). Because the dependence $\bar{N} = \bar{N}(W)$ cannot be determined in advance, this expression is best expanded into a series in W, which, when truncated to W^2, gives the following for the film resistance:

$$R = R_e + \frac{WR_r}{k_e \bar{N}_e}\left[\alpha + 2\beta(T_e - T_r)\right] - \frac{CW^2 R_r}{k_e \bar{N}_e} \times \left\{\alpha + \beta\left[2(T_e - T_r) - \frac{1}{Ck_e \bar{N}_e}\right]\right\} \tag{3}$$

where the $C = (1/\bar{N}_e)(\partial \bar{N}/\partial W)_e$ coefficient indicates the Nusselt number dependence on the power. If α, β, R_r, and T_r are available from an "oven" calibration as described, then Eq. (3) can be used to find the recovery factor $\eta = T_e/T_0$ in a flow of Mach number M, stagnation temperature T_0, and unit Reynolds number Re'. Figures 2 and 3 show η (Re', M, T_0) data for a typical probe, as always obtained by extrapolating data pairs W, R to zero power, reduced first by assuming $\beta = 0$ (see Fig. 2) and also by using the β found from the resistivity calibration (see Fig. 3). It is remarkable that, by accounting for $\beta \neq 0$, the η values shift significantly, and seeming influences of Re' and T_0 vanish. In addition, the recovery factor seems to decrease from 1 at $M = 0$ to about 0.945 at $M = 3$.

When the measured data pairs W, R are fitted by a quadratic polynomial in W, the coefficient of W in the polynomial can next be used to find $\bar{N}_e$, according to Eq. (3). Figure 4 plots the $\bar{N}_e$ vs Re' results from the same measurements giving the η data of Figs. 2 and 3. Within the scatter, and in the Re' range studied, these data were least-squares fitted by $\bar{N} = A\sqrt{Re'} + B$, independent of M as demonstrated in Fig. 4, with $A = 0.00565$ cm^2 and $B = 2.08$ cm. The effect of neglecting the β factor in Eq. (1) was to lower B by about 7%. The Mach number independence is explained by analogy with cylinder data[7,8] (hot wires), which show a Mach number dependence of $\bar{N}$ only for probe Reynolds numbers below about 10. By contrast a probe-height Reynolds number of several thousand results if the unit Reynolds numbers shown for the present tests are multiplied by a typical film height of 0.05 cm. Similar results of a Re'-independent η and a M-independent $\bar{N}$ have been reported by Seiner[9] for a commercial, wedge-type, hot-film probe suitable for lower temperatures.

In summary it is significant that, first, for film probes designed to withstand continuous exposure to hypersonic flow temperatures, the β coefficient in the resistance-temperature relation is apparently important; significant errors occur in the calibrations if β is neglected. Second, the inherently high Reynolds numbers of film probes remove the sensitivity to the

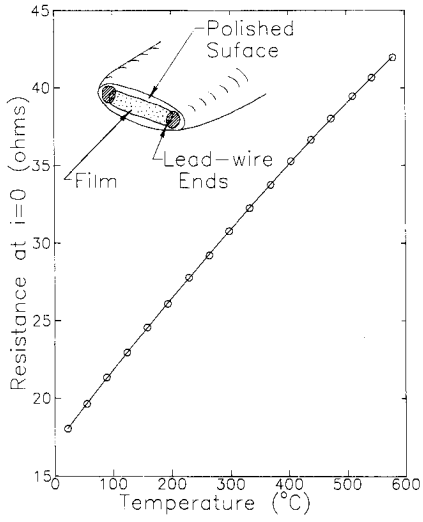

Fig. 1 Resistivity calibration of typical probe; solid line represents best second-degree fit of data.

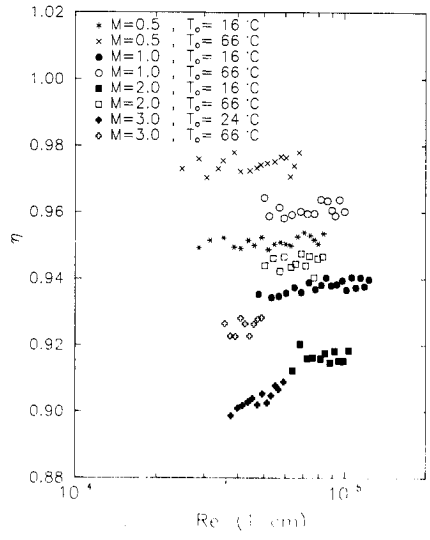

Fig. 2 Temperature recovery factor variation for typical probe; resistivity calibration with $\beta = 0$; R-W data fit with a second-degree polynomial.

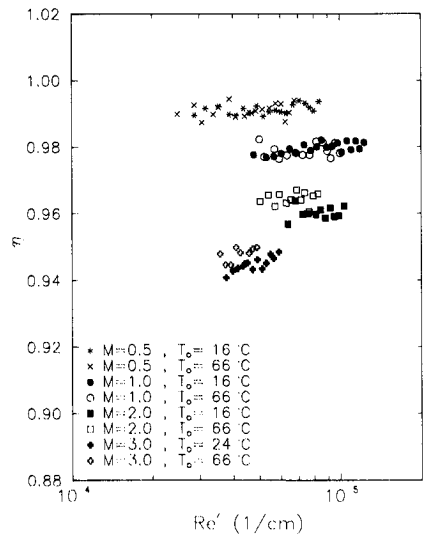

Fig. 3 Temperature recovery factor variation for typical probe; resistivity calibration with $\beta \neq 0$; R-W data fit with a second-degree polynomial.

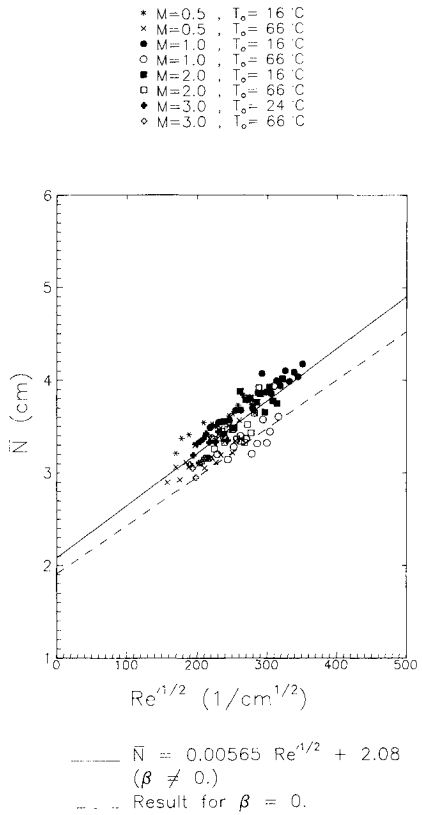

Fig. 4 Heat-transfer characteristics of typical probe; *R-W* data fit with a second-degree polynomial.

Mach number. If the derivatives $\partial\eta/\partial Re'$ and $\partial\bar{N}/\partial M$ can indeed be neglected while applying these probes to turbulence measurements, then the formulas needed to translate the probe alternating current signals to turbulence intensities[10] can be visibly simplified.

References

[1]Laderman, A. J., and Demetriades, A., "Turbulent Shear Stresses in Compressible Boundary Layers," *AIAA Journal*, Vol. 17, No. 7, 1979, p. 736.

[2]Demetriades, A., "Turbulence Measurements in an Axisymmetric Compressible Wake," *Physics of Fluids*, Vol. 11, No. 9, 1968, p. 1841.

[3]Demetriades, A., "New Experiments on Hypersonic Boundary Layer Stability Including Wall Temperature Effects," Heat Transfer and Fluid Mechanics Inst., Stanford Univ. Press, Stanford, CA, 1978, p. 39.

[4]Bellhouse, B. J., and Bellhouse, F. H., "Thin-Film Gauges for Measurement of Velocity or Skin Friction in Air, Water, or Blood," *Journal of Physics E.: Scientific Instruments*, Vol. 1, 1968, Series 2, pp. 1211-1213.

[5]Demetriades, A., Munger, C. O., and Anders, S. G., "Hot Film Anemometer Probes for High-Temperature Hypersonic Research," Montana State Univ., Bozeman, MT, MSU SWT TR 89 01, March 1989.

[6]Hinze, J. O., *Turbulence*, 1st ed., McGraw-Hill, New York, 1959, p. 78.

[7]Hertel, P. S., "Heat Transfer Characteristics of Small Configuration Hot-Wires in Low Reynolds Number Subsonic and Supersonic Air Flows," Master's Thesis, Montana State Univ., Bozeman, MT, March 1985.

[8]Dewey, C. F., Jr., "A Correlation of Convective Heat Transfer and Recovery Temperature Data for Cylinders in Compressible Flow," *International Journal of Heat and Mass Transfer*, Vol. 8, Feb. 1965, pp. 245-252.

[9]Seiner, J. M., "The Wedge Hot-Film Anemometer in Supersonic Flow," NASA TP-2134, May 1983, p. 56.

[10]Morkovin, M. V., "Fluctuations and Hot-Wire Aneomometry in Compressible Flows," AGARDograph 24, Paris, France, 1956.

Bending of Thick Angle-Ply Bimodular Composite Plates

Faramarz Gordaninejad*
University of Nevada, Reno, Reno, Nevada 89557

Introduction

A BIMODULAR (or bimodulus) material is one which behaves differently under tension and compression loads, and its nonlinear stress-strain curve is approximated by two straight lines: one in tension and the other in compression. Many fiber-reinforced composites, such as graphite/epoxy and tire-cord rubber exhibit this behavior. Within the last two decades, numerous investigations have been performed for isotropic and orthotropic beam, plate, and shell structures constructed from bimodular materials. In the following, only those studies related to the analysis of bimodular composite plates are briefly addressed. For a comprehensive review of the literature, readers are referred to a study by Bert and Reddy.[1]

Kamiya[2,3] studied the large deformation of thin, isotropic, clamped circular and rectangular plates using the finite-difference and Galerkin methods, respectively. Singh et al.[4] reported results for bending of a thin, isotropic bimodular plate as applied to rock mechanics. They determined the position of the neutral surface of the plate by setting the total in-plane shear force equal to zero. Bert and Kincannon,[5] Reddy and Choa,[6] Reddy and Bert,[7] and Bert et al.[8] extended Kamiya's work to the analysis of thick, orthotropic laminated bimodular plates. They utilized the fiber-governed compliance theory introduced by Bert[9] to determine the position of neutral surface. Later, they extended their studies to large deflection,[10] thermal stress,[11] vibration,[12] and transient response[13] of orthotropic, laminated, bimodular composite plates. Doong and Chen[14] addressed the problem of vibration of thick, orthotropic plates under combined bending and extensional stresses. Gordaninejad[15] studied the effect of shear deformation on bending of orthotropic, bimodular composite plates by implementing Reddy's higher-order consistent shear deformation theory.[16] Furthermore, he developed a finite element model for the analysis of single-layer, anisotropic, bimodular composite plates.[17,18]

In the present study, the model in Ref. 17 is extended to analyze laminated anisotropic bimodular composite plates. The shear-deformation effect is included by employing the plate theory of Yang et al.[19] The position of the neutral surface is determined by using the fiber-governed compliance theory.[9] Because of the dependency of the neutral surface on the generalized displacements and angle of fiber orientation, no closed-form solution can be obtained even for the simplest loading cases and boundary conditions. Therefore, the displacement finite element method is utilized to solve the problem.

Theory and Formulation

Consider a two-layer, angle-ply, antisymmetric, rectangular plate of constant thickness h with fibers oriented at arbitrary angles $(\theta/-\theta)$. A Cartesian coordinate system is set at the center of the plate's midsurface with the z axis normal to the midsurface. The total displacements U and V, presented in Eq. (1), vary linearly and transverse deflection W remains constant through the thickness of the plate:

$$U = u + z\psi_x; \qquad V = v + z\psi_y; \qquad W = w \tag{1}$$

Received March 31, 1989; revision received Nov. 27, 1989.

*Associate Professor, Mechanical Engineering Department.